Strain Rate Induced Strength Enhancement in Concrete: Much ado about Nothing?

Leonard E Schwer

Schwer Engineering & Consulting Services

Windsor CA USA

Summary:

When concrete impact and penetration simulations are discussed, the question of increased strength due to high strain rates arises. Many concrete material modelers cite and use the seminal work of Bischoff and Perry (1991), or the widely accepted standard reference for concrete Comite Euro-International du Beton (1993) or CEB for short. Bischoff and Perry amassed a large amount of concrete laboratory data addressing strain-rate induced Dynamic Increase Factors (DIF) or the ratio of the measured dynamic to quasi-static strength.

Figure 2 is taken from Bischoff and Perry (1991) and shows the large amount of data they collected, along with the strain-rate equations recommended in the CEB for two concrete strengths. The data shows a large amount of scatter in reported strength increases. The depicted CEB equations approximately bound the data.

The CEB recommended strain-rate induced strength increase equations are:

$$\begin{aligned} \text{DIF} = \frac{\hat{f}_c'}{f_c'} &= \left(\frac{\dot{\varepsilon}_d}{\dot{\varepsilon}_0} \right)^{1.026\alpha} \quad \text{for} \quad |\dot{\varepsilon}_d| \le 30 \text{ s}^{-1} \\ \text{DIF} = \frac{\hat{f}_c'}{f_c'} &= \gamma_s \left(\frac{\dot{\varepsilon}_d}{\dot{\varepsilon}_0} \right)^{1/3} \quad \text{for} \quad |\dot{\varepsilon}_d| > 30 \text{ s}^{-1} \\ \alpha &= \frac{1}{5 + 9\frac{f_c'}{f_0'}} \qquad \log\gamma = 6.156\alpha - 2 \end{aligned} \tag{1}$$

Where f_c' is the quasi-static unconfined compressive strength, $\hat{f}_c'$ is the dynamic unconfined compressive strength, $f_0' = 10$ MPa , $\dot{\varepsilon}_d$ is the strain rate, and $\dot{\varepsilon}_0 = 30 \times 10^{-6}$ s^{-1}.

Concerning the CEB equations, Bischoff and Perry state:

> "It should be noted that the sharp increase predicted at rates greater than 30/s is only tentative, and other recent recommendations [113][1] have also been made which disregard this effect for concrete strength in compression."

[1] Reinhardt, H. W., "Simple relations for the strain rate influence on concrete", in 'Darmstadt Concrete', edited by G. Konig, H.W. Reinhardt and J.C. Walraven, Vol. 2 (Institut ffir Massivbau, T.H. Darmstadt, 1987) pp. 203-211.

The data collected by Bischoff and Perry clearly indicates there is some measurable increase in unconfined compressive strength of concrete with increasing strain rate, and we can accept the CEB formula's as being representative of the data. However, the unanswered question is

> *"Does this unconfined compression data translate into the simulations of interest, e.g. blast and penetration of concrete targets, and in particular, do the strain-rate forms used in constitute models?"*

The above question is addressed in two parts:

1. What do simulations of dynamic *unconfined* compressive strength tests predict?
2. What do the corresponding simulations of dynamic *confined* compressive strength tests predict? And, what data, if any, can be used to verify these models.

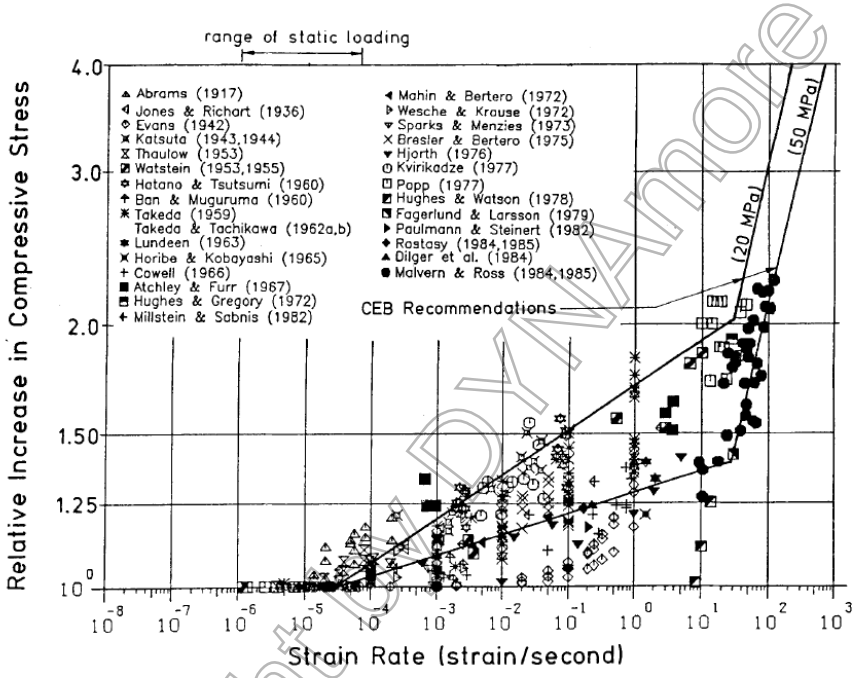

Figure 1 Log-log scale of strength increase versus strain rate showing data and CEB fits. (Figure 7 in Bischoff & Perry.)

Conclusions

Strain rate induced axial stress increases were produced in numerical simulations using a material model that does not explicitly include strain rate effects. The Dynamic Increase Factors observed in the simulations of unconfined and confined compression tests are similar to those reported in the literature for Split Hopkins Pressure Bar experiments (unconfined) and confined compression test.

Analysis of the simulation results indicates the Dynamic Increase Factors can be attributed to two factors:

1. At relatively low strain rates, i.e. less than 10/second, inertial confinement provides for axial stress increases of less than 20% in unconfined and confined compression simulations.
2. At higher strain rates, i.e. 100/second, the simulated specimens exhibited non-homogeneous lateral deformations. This lack of homogeneous deformations obviates the utility of the associated Dynamic Increase Factors for modeling the response continuum based constitutive behavior.

Keywords: Concrete, strain-rate, unconfined, confined

1 Background

When concrete impact and penetration simulations are discussed, the question of increased strength due to high strain rates arises. Many concrete material modelers cite and use the seminal work of Bischoff and Perry (1991), or the widely accepted standard reference for concrete Comite Euro-International du Beton (1993) or CEB for short. Bischoff and Perry amassed a large amount of concrete laboratory data addressing strain-rate induced Dynamic Increase Factors (DIF) or the ratio of the measured dynamic to quasi-static strength.

Figure 2 is taken from Bischoff and Perry (1991) and shows the large amount of data they collected, along with the strain-rate equations recommended in the CEB for two concrete strengths. The data shows a large amount of scatter in reported strength increases. The depicted CEB equations approximately bound the data.

The CEB recommended strain-rate induced strength increase equations are:

$$\begin{aligned} \text{DIF} &= \frac{\hat{f}_c'}{f_c'} = \left(\frac{\dot{\varepsilon}_d}{\dot{\varepsilon}_0}\right)^{1.026\alpha} \quad \text{for } |\dot{\varepsilon}_d| \le 30 \text{ s}^{-1} \\ \text{DIF} &= \frac{\hat{f}_c'}{f_c'} = \gamma_s \left(\frac{\dot{\varepsilon}_d}{\dot{\varepsilon}_0}\right)^{1/3} \quad \text{for } |\dot{\varepsilon}_d| > 30 \text{ s}^{-1} \\ \alpha &= \frac{1}{5 + 9\frac{f_c'}{f_0'}} \qquad \log\gamma = 6.156\alpha - 2 \end{aligned} \tag{2}$$

Where f_c' is the quasi-static unconfined compressive strength, $\hat{f}_c'$ is the dynamic unconfined compressive strength, $f_0' = 10$ MPa, $\dot{\varepsilon}_d$ is the strain rate, and $\dot{\varepsilon}_0 = 30 \times 10^{-6}$ s^{-1}.

Concerning the CEB equations, Bischoff and Perry state:

> "It should be noted that the sharp increase predicted at rates greater than 30/s is only tentative, and other recent recommendations [113][2] have also been made which disregard this effect for concrete strength in compression."

The data collected by Bischoff and Perry clearly indicates there is some measurable increase in unconfined compressive strength of concrete with increasing strain rate, and we can accept the CEB formula's as being representative of the data. However, the unanswered question is

> *"Does this unconfined compression data translate into the simulations of interest, e.g. blast and penetration of concrete targets, and in particular, do the strain-rate forms used in constitute models?"*

The above question is addressed in two parts:

3. What do simulations of dynamic *unconfined* compressive strength tests predict?
4. What do the corresponding simulations of dynamic *confined* compressive strength tests predict? And, what data, if any, can be used to verify these models.

[2] Reinhardt, H. W., "Simple relations for the strain rate influence on concrete", in 'Darmstadt Concrete', edited by G. Konig, H.W. Reinhardt and J.C. Walraven, Vol. 2 (Institut ffir Massivbau, T.H. Darmstadt, 1987) pp. 203-211.

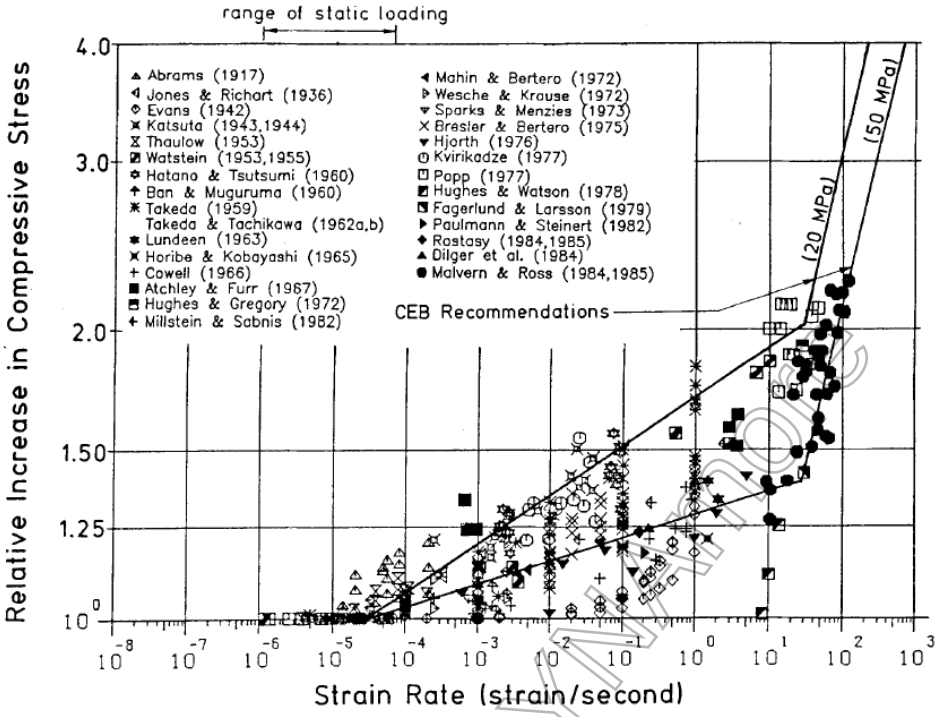

Figure 2 Log-log scale of strength increase versus strain rate showing data and CEB fits. (Figure 7 in Bischoff & Perry.)

2 Dynamic Unconfined Compressive Strength Tests

Recent work by Li & Meng (2003) and Zhou & Hao (2008) provide computational confirmation of inertial confinement contributing to the observed increase in dynamic strength in unconfined compression tests, as outline by Bischoff and Perry (1993).

What is inertial confinement? If a quasi-static load is applied in an unconfined compression test, the lateral surfaces of the cylindrical specimen are free to expand under the action of Poisson's effect, and the specimen remains in a state of plane stress. However, if the same test is performed dynamically, there will be a delay in the radial expansion of the outer cylinder as the material (mass) must first be accelerated in the radial direction. The delay in the lateral surface reaching a static equilibrium position, e.g. zero radial stress, results in an effective confining pressure on the lateral surfaces of the specimen. Hence the term inertial confinement.

In a quasi-static unconfined compression tests, the stress difference and mean stress are related by:

$$\begin{aligned} SD &= \sigma_1 - \sigma_3 = \sigma_1 = 3p \\ p &= \left(\sigma_1 + 2\sigma_3\right)/3 = \sigma_1/3 \end{aligned} \tag{3}$$

For a dynamic unconfined compression test, the mean stress will be greater than the corresponding quasi-static value, p, due to the presence of the inertial confinement. The corresponding stress trajectories in stress difference versus mean stress space are shown in Figure 3. Because concrete, and all geomaterials, are frictional materials, i.e. their shear strength increases with increasing confinement, there will be an apparent increase in the dynamic strength of the material relative to the quasi-static strength.

Another way to think of inertial confinement is that the stress trajectory changes from plane stress in quasi-static loading to approaching plane strain in high strain-rate loading. Plane strain is often

assumed in so call gas gun flyer-plate experiments, used to investigate the high strain rate response of materials, where the specimen is relative thin with respect to its diameter, i.e. disk like.

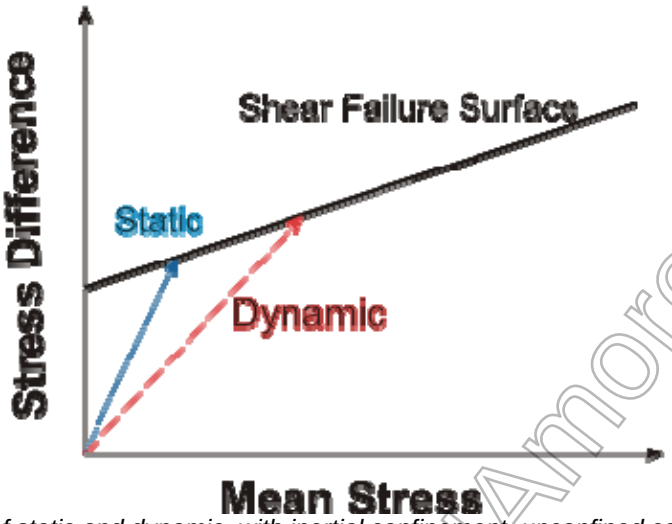

Figure 3 Schematic of static and dynamic, with inertial confinement, unconfined compression test.

In metals, the corresponding shear failure surface would be a horizontal line, because the uniaxial yield strength of metals is independent of confining stress. Thus, to obtain a strain-rate effect in metals, the shear failure surface is modeled as translating (hardening) in the vertical direction.

The same type of stain-rate hardening induced translation of the shear failure surface for concrete is assumed in some concrete constitutive models. The question to be answered is:

"How much of the observed increase in strength is due to inertial confinement and home much is due to the strain-rate hardening of the shear failure surface?"

3 Unconfined Compression Test Simulations

In this section unconfined compression tests are simulated both quasi-statically and dynamically using a concrete constitutive model that does not include explicit strain-rate effects, e.g. similar to those recommended by the CEB. By omitting constitutive model strain-rate effects, i.e. strain-hardening of the shear failure surface, a numerical assessment of the inertial confinement effects can be established. Further, these dynamic unconfined compression results can then be compared directly to the CEB recommendations, and by inference to the data of Bischoff and Perry (1991).

3.1 Quasi-Static Simulation

Figure 4 shows a cut away view of the cylindrical model used in the numerical simulations. The specimen is a right circular cylinder of diameter 400 mm and height 400 mm comprised of 920 solid (8 node hexahedra) elements with approximate dimensions of 40x40x40 mm. The specimen is loaded along the upper circular surface via normal to the surface prescribed velocity. The magnitude of the velocity, v, is chosen to provide a nominal strain rate, $\dot{\varepsilon}$, in the axial direction:

$$\dot{\varepsilon} = \frac{\varepsilon}{\Delta t} = \frac{1}{\Delta t}\frac{\Delta L}{L} = \frac{1}{L}v \qquad (4)$$
$$v = L\dot{\varepsilon}$$

For the quasi-static case, the strain rate is set to $10^{-4}\ \mathrm{ms}^{-1} = 0.1\ \mathrm{s}^{-1}$. Although this strain rate is slightly above the quasi-static range indicted in Figure 2, i.e. $10^{-4}\ \mathrm{s}^{-1}$, as will be demonstrated, the

simulation result reproduces the static unconfined compressive strength, so lower values of strain rate were not deemed necessary.

The bottom circular surface of the specimen is constrained from motion in the axial direction of the cylinder and the lateral surface is traction free.

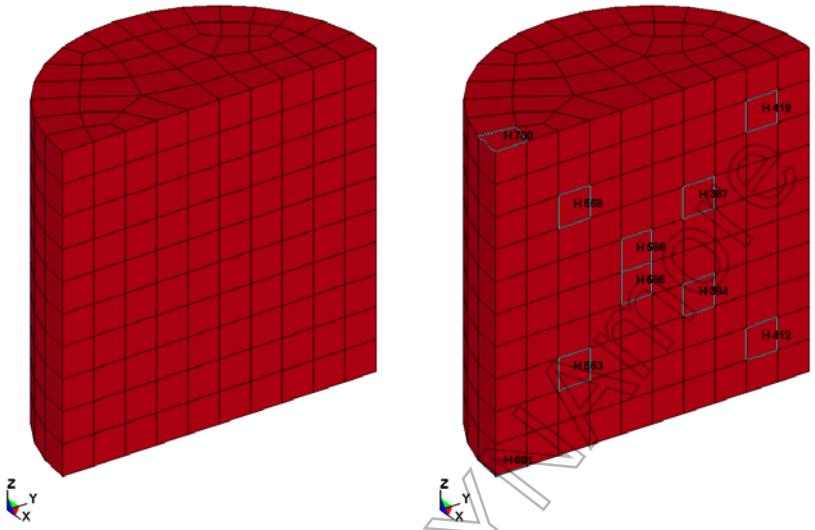

Figure 4 Cut away view (half) of model for simulation of unconfined compression tests.

The concrete is modeled using the LS-DYNA Pseudo-TENSOR (MAT016) model. The inputs are the unconfined compressive strength, 45.6 MPa, the elastic shear modulus, 4.6 GPa, Poisson's ratio, 0.1, and the mass density, 2.17×10^{-3} g/mm^3. The model internally generates the shear failure surface and the pressure-volume response.

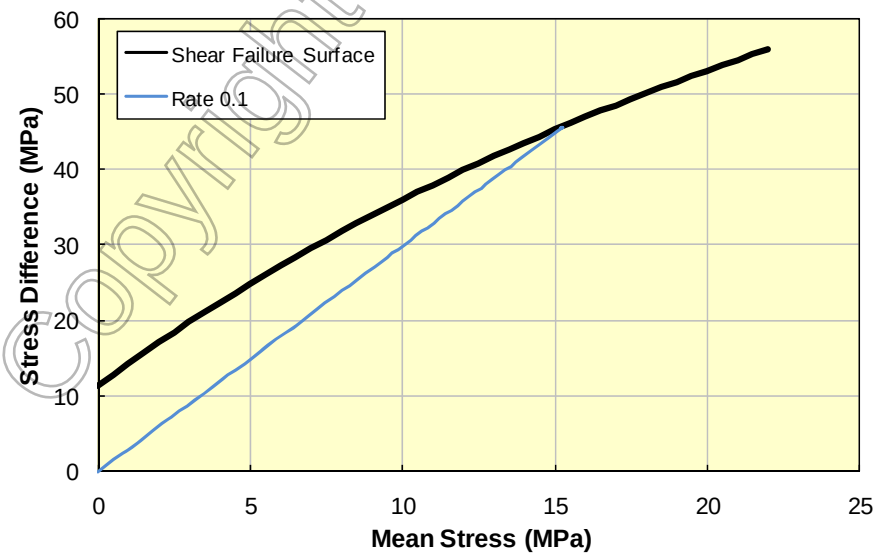

Figure 5 Quasi-static (strain rate 0.1/s) stress difference versus mean stress unconfined compression test simulation.

Figure 5 shows the average stress difference (same as the von Mises stress) versus the average mean stress for the unconfined compression test simulation; the averages are formed using the 10

elements indicated in right side image of Figure 4. Also shown is the shear failure surface generated by MAT016 for an unconfined compressive strength of 45.6 MPa.

The maximum stress difference in this simulation is 45.6 MPa, as expected. Also as indicated in Equations (3), this is the maximum axial stress in the specimen. Note: although the specimen continues to deform (strain) no additional axial stress can be carried by the specimen since the material model assumes elastic-perfectly plastic behavior.

Another way to assess the maximum axial stress is to monitor the reaction force at the bottom circular surface of the specimen. This reaction force, divided by the cylinder cross section area, provides the engineering stress. Figure 6 shows this axial stress history for the quasi-static loading case. This axial stress history indicates the simulation is quasi-static as there is no overshooting of the unconfined compressive strength, nor oscillations in the stress after the shear failure surface is reached.

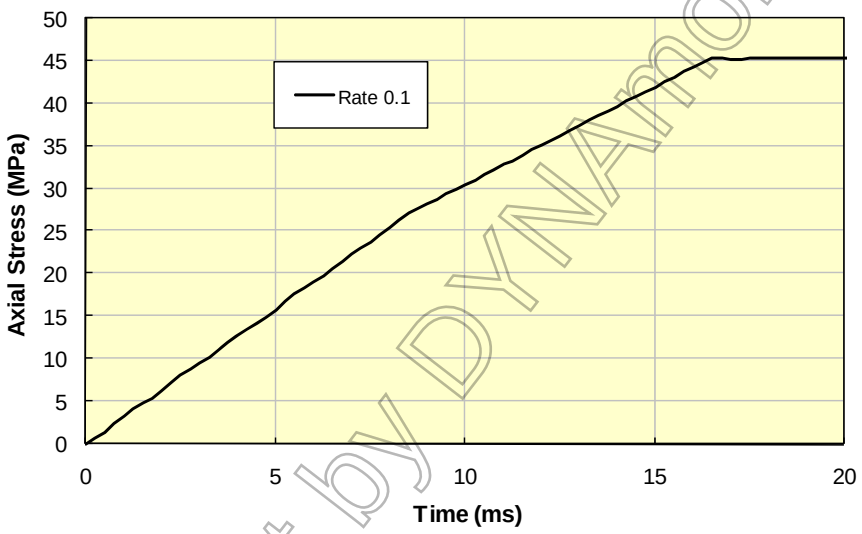

Figure 6 Axial stress history at bottom of cylinder, obtained from axial reaction force.

3.2 Dynamic Simulations

The results shown in Figure 5 and Figure 6 are taken to represent the quasi-static behavior of the unconfined compression test simulation. In this section, a demonstration of how these unconfined compression test simulation responses change as the strain-rate is increased.

Figure 7 compares the stress difference versus mean stress response of the quasi-static case, shown previously in Figure 5, with the corresponding simulation results when the axial strain rate is increased to a nominal value of 10/second. At the higher nominal strain rate of 10/s the stress trajectory essentially follows the quasi-static stress trajectory, up to the shear failure surface. When the shear failure surface is reached, the higher strain rate stress trajectory is able to follow the shear failure surface to greater values of the stress difference. This is because the inertial confinement is providing additional lateral pressure to the simulated specimen. For this strain rate, the maximum stress difference attained is 49 MPa, before the specimen unloads along the shear failure surface as the lateral inertial pressure (over) relaxes due to expansion of the cylinder. Note: this maximum stress difference is not equal to the maximum axial stress, since obviously the mean stress is no longer one-third of the axial stress as in a quasi-static simulation.

Increasing the nominal strain by a factor of 10, i.e. to 100/second, results in the stress difference versus mean stress comparison shown in Figure 8. At the nominal strain rate of 100/s the average stress difference versus average mean stress trajectory no longer intersects the shear failure surface,

but appears to parallel the shear failure surface. This change in behavior is because now the deformation of the simulated unconfined compression specimen is no longer homogeneous (uniform).

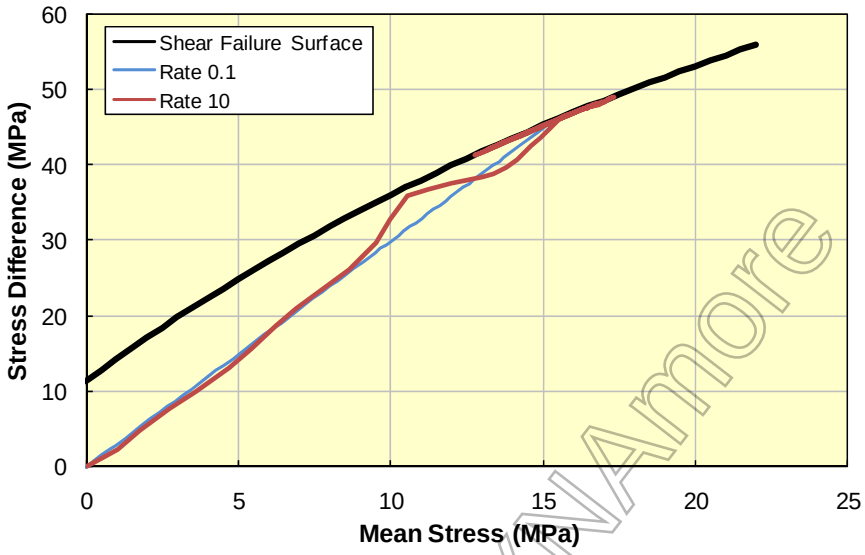

Figure 7 Stress difference versus mean stress comparison of quasi-static and increased strain rate, 10/s, unconfined compression test simulation results.

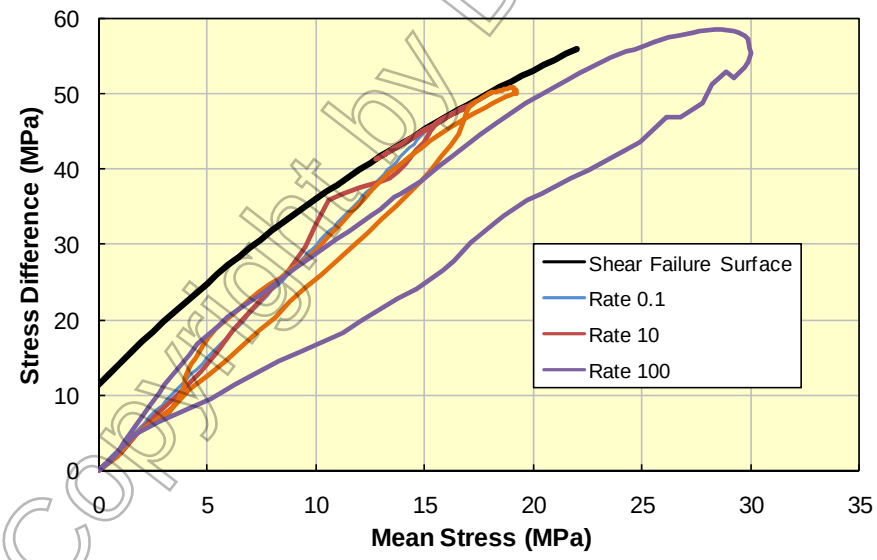

Figure 8 Stress difference versus mean stress comparison of quasi-static and increased strain rates of 10/s and 100/s for a simulated unconfined compression test.

Indications of the lack of homogeneity in the specimen are shown in Figure 9 where fringes of pressure are shown at a time of 0.148 ms as the axial stress wave reflects from the fix bottom of the model. These pressure fringes also clearly indicate the central core of the specimen maintains a large mean stress, about 30 MPa, although the pressure at the outer surface is significantly lower. The large core pressures are the result of inertial confinement by the outer region of the specimen.

As further evidence of the non-uniform deformation of the simulated unconfined compression test specimen, the deformed shape of the specimen at the end of the simulation is also shown in Figure 9, with the displacements magnified by a factor of 3. Clearly the top of the specimen is expanding in the radial direction more than the bottom of the specimen.

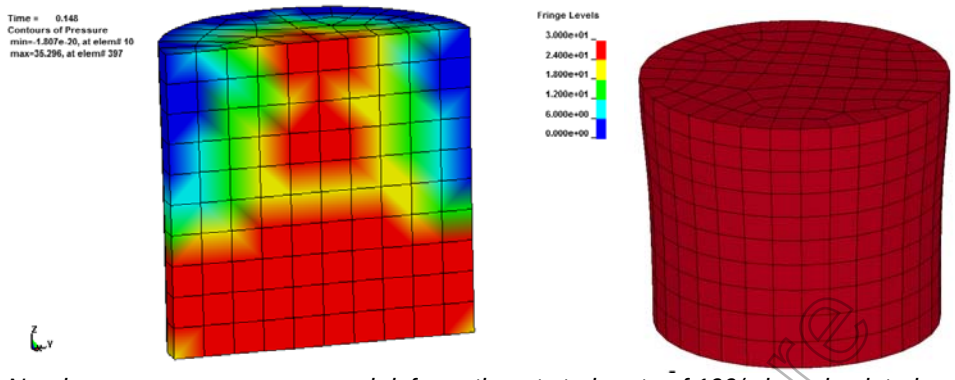

Figure 9 Non-homogeneous pressure and deformation at strain rate of 100/s in a simulated unconfined compression specimen.

As the strain rate is increased, using the average stress difference is no longer an accurate measure of the maximum axial stress, since the deformation is no longer homogeneous and the increased inertial pressure provides for a reduced stress difference. Figure 10 compares the axial stress obtained from the reaction force at the bottom of the cylinder for the three strain rates considered. This method of assessing the increasing axial stress with increasing strain rate is comparable with measurements that would be made in laboratory tests conducted in a tri-axial testing machine that used a load cell. As shown in Figure 10, the maximum axial force for three selected strain rates of 1, 10 and 100/s are 46.2, 52.2 and 74.9 MPa, respectively. Recall the quasi-static strain of 0.1/s produced a maximum axial force of 45.6 MPa, equal to the unconfined compression strength.

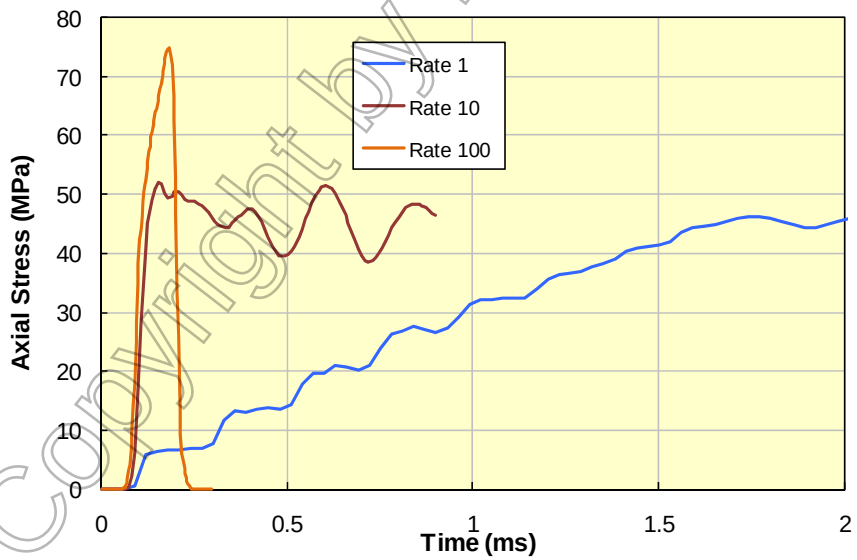

Figure 10 Axial stress histories obtained from the reaction force at bottom of simulated specimen.

3.3 Comparison with SHPB Data and Simulations

Figure 11 presents a comparison of the unconfined compression test simulation results discussed above[3], with Split Hopkins Pressure Bar (SHPB) data as reported by Li & Meng (2003), and their SHPB simulation results. The data consists of:

[3] Additional unreported simulation results at intermediate and higher strain rates are included.

- The concrete data reported by Malvern and Ross (1985),
- The concrete data reported by Tedesco & Ross (1998),
- The mortar data reported by Grote et al. (2001).

For completeness, the fits to the data reported by Li & Meng are included in an appendix.

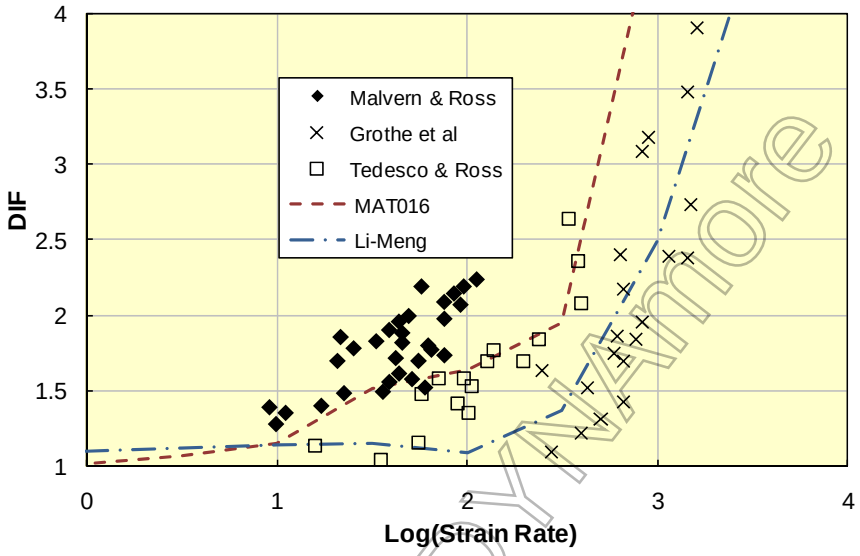

Figure 11 Comparison of MAT016 axial stress dynamic increase factor (DIF) with SHPB laboratory data, and Li & Meng simulation results.

The results shown in Figure 11 indicate that the two simulation results, i.e. MAT016 and Li-Meng, which do not include explicit strain-rate effects, exhibit increasing strength with increasing strain rate. Note: the MAT016 results are dynamic unconfined compression test simulations and not SPHB simulations.

The majority of the data shown in Figure 11 was obtained at strain rates greater than 100/s. As noted above, in the unconfined compression test simulations, the specimen deformation was no longer uniform at strain rates of 100/s or greater. There is a possibility the test data also reflects non-homogeneous deformation of the laboratory specimens. A lack of homogeneous deformations would obviate the use of the such strain rate data to characterize a continuum based material model.

4 Confined Compression Test Simulations

The focus of the concrete strain rate literature is on unconfined compression, and tension, tests. However, for practical applications such states of stress rarely exist. The typical application involves large concrete structures subjected to blast, impact or penetration. In these applications the concrete subject to the highest strain rates is often well confined by surrounding concrete, and sometime reinforcement. Thus the practical question is:

"What is the effect of strain rates on confined concrete specimens?

4.1 Available Confined Compression Strain Rate Data

This question of the effect of confinement on strain rate effects was addressed by Bischoff and Perry (1991) in their Section 2.2 "Multi-axial Loading: Strain-Rate Influence," referring to confined dynamic tests performed by Takeda et a. (1974) and Yamaguchi et al. (1989):

> *"The failure envelope moved upwards at higher loading rates but merged into one unique envelope when the octahedral shear and normal stresses were normalized with the uniaxial compressive strength corresponding to the loading rate involved."*

The data referred to had statically applied initial confinements of up to 30 MPa and 90 MPa, respectively, with maximum strain rates of 2/s quoted for the Takeda et a. data. From the CEB equations, and data shown previously in Figure 11, at strain rate of 2/s, the unconfined strength increase is about 1.3.

This factor of 1.3 is also consistent with the data by Gran et al. (1989), who reported a 30 to 40% increase in the dynamic failure envelope of a 40 MPa concrete, over the corresponding static failure envelope of strain rates of 2/s.

In summary, the limited strain rate data available on dynamic confined compression tests, i.e. up to 2/s, indicates the shear failure surface is shifted (increased) by about the same factor (DIF) as found in the unconfined compression tests. No data is presently available to extend this conclusion much beyond strain rates of 2/s, which is lower than the range of interest for practical applications.

4.2 Quasi-Static & Dynamic Simulations

Confined compression simulations were performed with the same model, both geometry and material, as described in the previous section for the unconfined compression test simulations. The model specimen was loaded hydrostatically, to the prescribed confining pressure of 5, 10, 20 and 40 MPa, and then the top surface of the model was prescribed a velocity to produce the nominal strain rate.

The nominal strain rates simulated were 0.1, 1, 10 and 100/second. The two lower strain rates produced nearly identical results at all four confinement levels, and are assumed to be slow enough to represent the quasi-static results. Note: the currently available data for dynamics confined compression tests is for somewhat larger confinements, but at a strain rate of 2/second.

Table 1 summarizes the Dynamic Increase factors (DIF) results from the dynamic confined compression test simulations. As was done previously, the axial stress was obtained by dividing the total force at the bottom (fixed end) of the cylinder by the circular area. The values in Table 1 are the maximum axial stress recorded during the simulation.

Table 1 Summary of Dynamic Increase Factors for confined compression test simulations.

Confinement (MPa)	Axial Stress Static (MPa)	DIF		
		1/s	10/s	100/s
5	64.8	1.00	1.08	1.48
10	78.7	1.00	1.09	1.78
20	100.2	1.00	1.10	1.31
40	127.6	1.05	1.09	1.30

The large Dynamic Increase Factors that occur at a nominal strain rate of 100/second are associated with non-homogeneous deformation of the simulated specimen, as illustrated in Figure 12. This figure shows the deformed shape of the cylindrical specimen at the end of the simulation with the deformations scaled by a factor of 3. Both the 5 and 40 MPa confinement specimens have uniform deformation at a nominal strain rate of 10/second. However, the same two confinement cases exhibit significant localized lateral deformations (top of specimen) at a nominal strain rate of 100/second. This is similar to the non-uniform deformations noted for the unconfined compression simulations.

Figure 13 shows the axial stress histories, obtained from the force at the bottom of the specimen, for the 40 MPa confinement dynamic compression simulation. Note: the maximum axial stress, used in calculating the DIF, exisits for a very short duration, and that the longer duration stress is oscillating about a value much closer to the quasi-static axial stress value. If the longer term axial stress values were used to determine the DIF, the factors would be less than 1.10 for the strain-rates of 1, 10 and 100/second.

5 Conclusions

Strain rate induced axial stress increases were produced in numerical simulations using a material model that does not explicitly include strain rate effects. The Dynamic Increase Factors observed in the simulations of unconfined and confined compression tests are similar to those reported in the literature for Split Hopkins Pressure Bar experiments (unconfined) and confined compression test.

Analysis of the simulation results indicates the Dynamic Increase Factors can be attributed to two factors:

3. At relatively low strain rates, i.e. less than 10/second, inertial confinement provides for axial stress increases of less than 20% in unconfined and confined compression simulations.
4. At higher strain rates, i.e. 100/second, the simulated specimens exhibited non-homogeneous lateral deformations. This lack of homogeneous deformations obviates the utility of the associated Dynamic Increase Factors for modeling the response continuum based constitutive behavior.

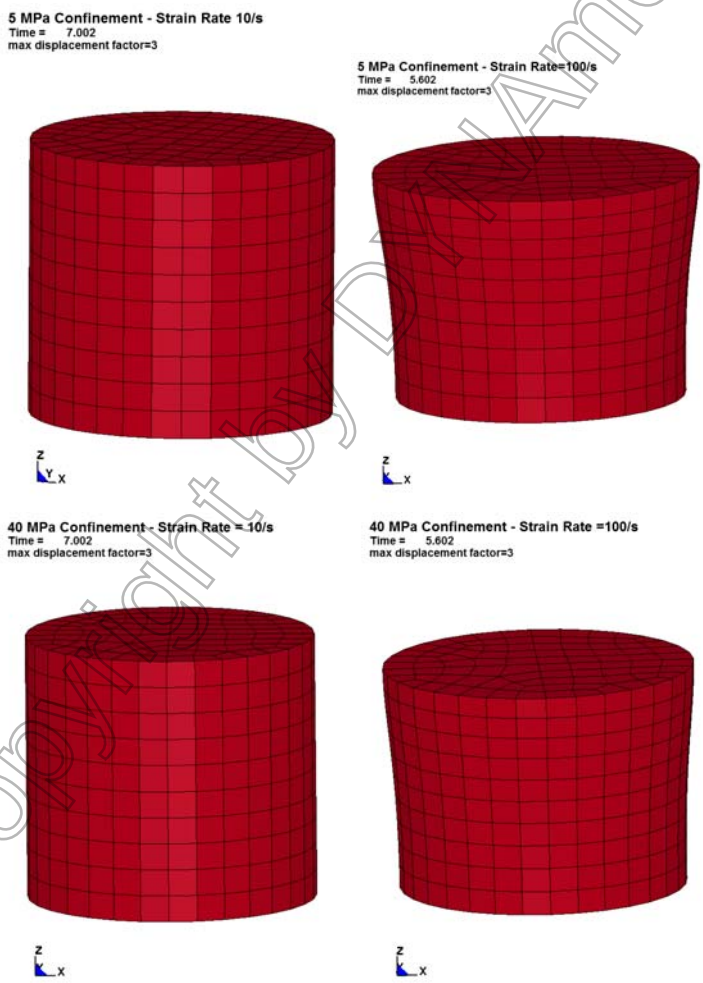

Figure 12 Magnified by a factor of 3 deformed shapes of 5 MPa (top row) and 40 MPa (bottom row) confined compression simulations at nominal strain rates of 10/s (left column) and 100/s (right column).

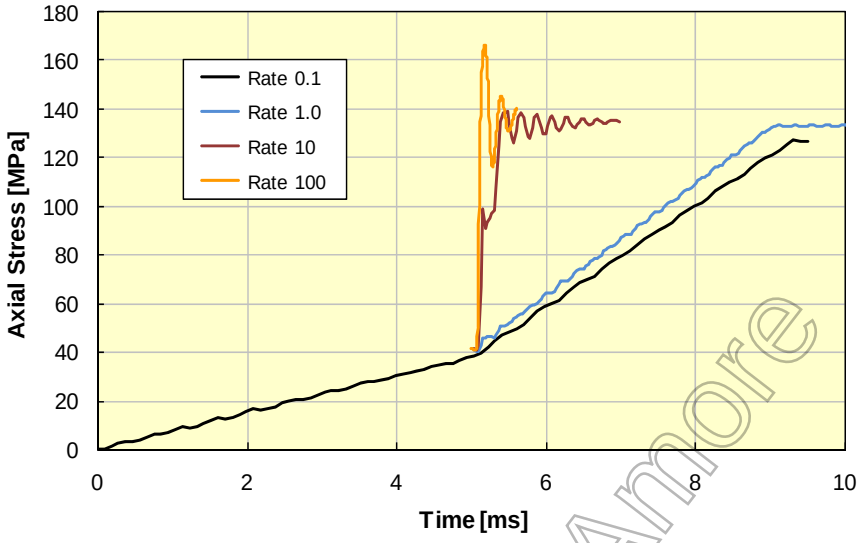

Figure 13 Axial stress histories for 40 MPa confinement dynamic compression test simulations.

6 References

Bischoff, P.H., Perry, S.H., "Compression behavior of concrete at high strain-rates," *Materials and Structures,* Volume 24, pages 425–450, 1991.

Comite Euro-International du Beton, *CEB-FIP model code 1990*, Redwood Books, Trowbridge, Wiltshire, UK, 1993.

Li, Q.M. and H. Meng, "About the dynamic strength enhancement of concrete-like materials in a split Hopkinson pressure bar test," *International Journal of Solids and Structures,* Volume 40, pages 343–360, 2003.

Zhou, X.Q. and H. Hao, "Modelling of compressive behaviour of concrete-like materials at high strain rate," *International Journal of Solids and Structures,* Volume 45, pages 4648–4661, 2008.

Malvern, L.E. and C.A. Ross, "Dynamic response of concrete and concrete structures," Second Annual Technical Report, AFOSR Contract No. F49620-83-K007 1985.

Tedesco, J.W. and C.A. Ross, "Strain-rate-dependent constitutive equations for concrete," ASME Journal of Pressure Vessel Technology, Volume 120, pages 398–405, 1998.

Grote, D.L., S.W. Park, and M. Zhou, "Dynamic behavior of concrete at high strain-rates and pressures: I. Experimental characterization," *International Journal of Impact Engineering*, Volume 25, pages 869–886, 2001.

Takeda, J., H. Tachikawa, and K. Fujimoto, "Mechanical Behaviour of Concrete Under Higher Rate Loading than in Static Tests," in *Mechanical Behaviour of Materials*, Volume 2, Society of Materials Science, Kyoto, pages 479-486, 1974.

Yamaguchi, H., K. Fujimoto and S. Nomura, "Strain Rate Effect on Stress-Strain Relationships of Concrete," in Proceedings of 4th Symposium on the Interaction of Non-Nuclear Munitions with Structures, Florida, pages290-295, 1989

Gran, J. K., A.L. Florence and J.D. Colton., "Dynamic Triaxial Tests of High-Strength Concrete," ASCE Journal Engineering Mechanics, Volume 115, Number 5, pages 891-904, 1989.

7 Appendix – Other Fits to Concrete Strain Rate Data

This appendix reproduces the Split Hopkins Pressure Bar data, and fits, as reported by Li & Meng (2003). The data and fits are illustrated in Figure 14, and the subsequent equations provide the analytical fits to the laboratory data.

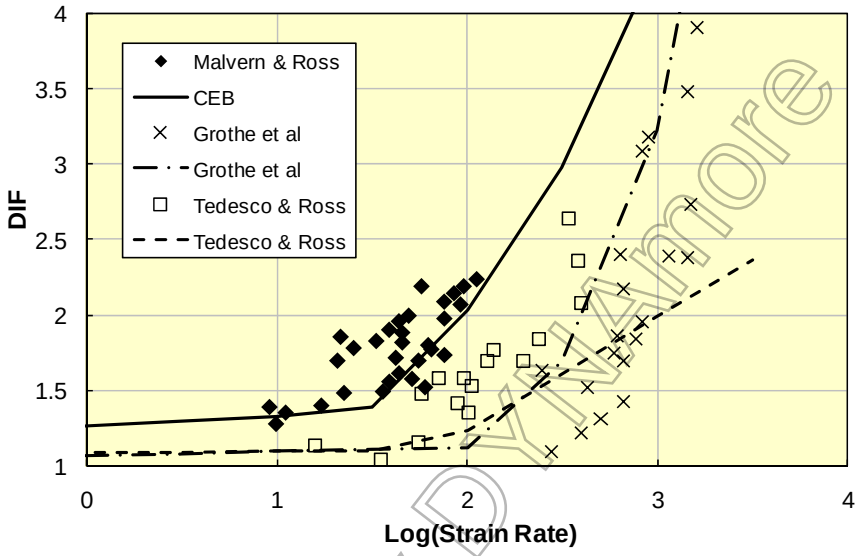

Figure 14 Split Hopkins Pressure bar data and fits as reported by Li & Meng (2003).

7.1 Split Hopkins Bar Data of Tedesco & Ross (1998)

$$\begin{aligned} \text{DIF} &= \frac{\hat{f}_c'}{f_c'} = 0.00965 \log \dot{\varepsilon}_d + 1.058 \geq 1.0 \quad \text{for} \quad \dot{\varepsilon}_d \leq 63.1 \text{ s}^{-1} \\ \text{DIF} &= \frac{\hat{f}_c'}{f_c'} = 0.758 \log \dot{\varepsilon}_d - 0.289 \leq 2.5 \quad \text{for} \quad \dot{\varepsilon}_d > 63.1 \text{ s}^{-1} \end{aligned} \tag{5}$$

7.2 Split Hopkins Bar Data of Grote et al. (2001)

$$\begin{aligned} \text{DIF} &= \frac{\hat{f}_c'}{f_c'} = 0.0235 \log \dot{\varepsilon}_d + 1.07 \quad \text{for} \quad \dot{\varepsilon}_d \leq 266 \text{ s}^{-1} \\ \text{DIF} &= \frac{\hat{f}_c'}{f_c'} = 0.822 \left(\log \dot{\varepsilon}_d\right)^3 - 4.4 \left(\log \dot{\varepsilon}_d\right)^2 + 7.22 \log \dot{\varepsilon}_d - 2.64 \quad \text{for} \quad \dot{\varepsilon}_d > 266 \text{ s}^{-1} \end{aligned} \tag{6}$$

7.3 Numerical Results of Li & Meng (2003)

$$\mathrm{DIF} = \frac{\hat{f}'_c}{f'_c} = 0.03438\left(3 + \log \dot{\varepsilon}_d\right) + 1 \quad \text{for} \quad \dot{\varepsilon}_d \le 100 \text{ s}^{-1}$$
$$\mathrm{DIF} = \frac{\hat{f}'_c}{f'_c} = 1.729\left(\log \dot{\varepsilon}_d\right)^2 - 7.1372 \log \dot{\varepsilon}_d + 8.5303 \quad \text{for} \quad \dot{\varepsilon}_d > 100 \text{ s}^{-1} \tag{7}$$